JOURNAL OF SOLID STATE CHEMISTRY 108, 152–157 (1994)

Solid-State Reaction Kinetics Determination via *in Situ* Time-Resolved X-Ray Diffraction

K. M. Forster, J. P. Formica, J. T. Richardson,[1] and D. Luss[1]

University of Houston, Department of Chemical Engineering, Houston, Texas 77204-4792

Received February 1, 1993; in revised form May 11, 1993; accepted May 13, 1993

Novel sample preparation and data reduction techniques were used to determine quantitative phase abundances from *in situ* time-resolved X-ray diffraction data and to follow the rate of solid-state reactions. This is illustrated by a study of the formation of $YBa_2Cu_3O_6$ from an intimate mixture of $BaCO_3$, CuO, and Y_2O_3 under controlled atmospheres. Thin layers of precursor powder were used as samples to minimize thermal gradients and obtain suitable data for Rietveld refinement. The mass fractions of the reacting phases were determined by comparing the integrated intensities of selected reflections acquired over short time intervals during the reaction to those at the end of the reaction. Phase abundances were quantified via Rietveld refinement of room-temperature diffraction data taken upon completion of the reactions.

INTRODUCTION

Traditional kinetic studies of solid-state reactions use thermogravimetry and differential thermal analysis, while X-ray diffraction has usually been limited to phase identification. When simultaneous reactions occur, thermal analysis can be inconclusive without a priori knowledge of the reaction pathways and any phase transformations (1–3). Early X-ray kinetic studies were made *ex situ* by removing the sample from the furnace, quenching, and then taking a diffraction pattern (4). Abundances (mass fractions) of the crystalline phases were estimated from relative heights of the Bragg reflections. This approach hinges on assumptions that frequently produce incorrect values of the phase abundances. Moreover, intermediate, metastable phases that decompose under ambient conditions are not observed in the diffraction pattern, leading to additional errors.

The diffracted intensities of a crystalline phase are proportional to the number of irradiated unit cells, which changes during reaction (5). Variations in phase abundance may be followed by measuring changing intensities. Several effects complicate high-temperature measurements, including broadening of the diffraction peaks due to small crystallite size (5), sample thermal expansion, and intensity damping due to increased thermal vibrations. These problems are generally corrected with longer counting times, but kinetic studies require rapid data collection.

In a standard measurement, a scintillation detector collects intensities at angular intervals of a few hundredths of a degree. This is time consuming, even when scanning over a few degrees. Until recently, *in situ* X-ray diffraction with a sealed-tube source has been limited to the study of equilibrium states or slowly reacting systems. The advent of fast detection systems, such as area detectors and position sensitive detectors (PSD), enables time-resolved studies of solid-state reactions with standard laboratory X-ray sources (6). In this work, novel sample preparation and data reduction techniques were applied to the problem of extracting quantitative phase abundances from time-resolved *in situ* X-ray data.

BACKGROUND

The diffracted intensity of a reflection (*hkl*) from a non-infinitely thick powder sample is (5).

$$I_j(\theta) = |SF_j(\theta)DW_j(\theta)|^2 * M_j(hkl) * A_v(\theta) * LP(\theta)/V_j^2, \quad [1]$$

where subscript j denotes the phase, $SF_j(\theta)$ is the structure factor, $DW_j(\theta)$ the Debye–Waller temperature factor, $M_j(hkl)$ the multiplicity factor, $A_v(\theta)$ the absorption factor, $LP(\theta)$ the polarization factor, and V_j the unit cell volume. The structure factor is given by (5)

$$SF(\theta) = \sum_i f_i * \exp\left(\frac{-i2\pi \sin\theta \cdot r_i}{\lambda}\right), \quad [2]$$

where the sum is over every atom in the unit cell, f_i is the atomic form factor of atom i, and r_i locates atom i in the unit cell. The atomic form factor of an element is

[1] To whom correspondence should be addressed.

0022-4596/94 $6.00

approximately equal to the atomic number for small θ, so phases with heavy elements diffract X-rays more intensely than those with light elements. In high-temperature experiments, the structure factor for a given reflection can change dramatically as the atoms adjust their positions within the unit cell during thermal expansion. As such, comparisons between relative intensity and phase abundance may cause large errors.

For a mixture of crystalline phases, the integrated intensity I_{ij} of reflection i of phase j satisfies the relationship (5)

$$I_{ij} \propto \frac{X_j * I_i}{\rho_j \left(\frac{\mu'}{\rho}\right)_m}, \quad [3]$$

where X_j is the mass fraction, I_i the calculated intensity of reflection i of a single-phase j sample, ρ_j the theoretical density, and μ'_m the linear absorption coefficient of the mixture. The mass absorption coefficient of the mixture $(\mu'/\rho)_m$ is given by

$$\left(\frac{\mu'}{\rho}\right)_m = \sum_j \frac{\mu_j}{\rho_j} X_j. \quad [4]$$

Standard quantitative analysis techniques typically require addition of an analyte that produces no preferred orientation or microabsorption effects. By adding a known amount of standard analyte, the mass fractions in a mixture can be determined from intensity ratios of selected strong reflections. In addition, the analyte must have strong reflections that neither overlap reflections from the mixture nor react with it. It is undesirable to add an analyte to a reacting system because its presence could alter the reaction pathways and kinetics. The Chung method uses no analyte but requires that the ratio of intensities for a known mass ratio of the constituent phases be known (7). For accurate results this method requires several strong, nonoverlapping reflections for each phase.

In this work, the mass fractions were determined from a diffraction pattern by Rietveld refinement (8). The diffracted intensity at any angle is given by (9)

$$I_t(\theta) = I_b(\theta) + \sum_{i,j} I_{ij}(\theta') H_j(\theta - \theta'), \quad [5]$$

where $I_b(\theta)$ is the background intensity, $I_{ij}(\theta)$ is the intensity of reflection i of phase j, and $H_j(\theta - \theta')$ is a peak profile function with θ' corresponding to the position of a Bragg reflection. A Rietveld refinement minimizes the difference between the measured diffraction and calculated patterns via Eq. [5] in a least-squares sense.

Determining the phase abundances as a function of time is the main goal in kinetic measurement. In this study, samples were quenched at 20°C/sec once the system approached equilibrium. No statistically significant change in the diffraction pattern was observed upon quenching during test experiments. At room temperature, scans were measured from 10–90° 2θ at 0.25° 2θ/min, and these data are refined. The $X_j(t_{final})$ factors obtained from the refinement correspond to the integrated intensities of the final high-temperature scan. Assuming no mass loss during the reaction, the mass fraction $X_j(t)$ is then given by:

$$X_j(t) = X_j(t_{final}) \frac{\sum_{hkl} I_j(hkl, t)}{\sum_{hkl} I_j(hkl, t_{final})}, \quad [6]$$

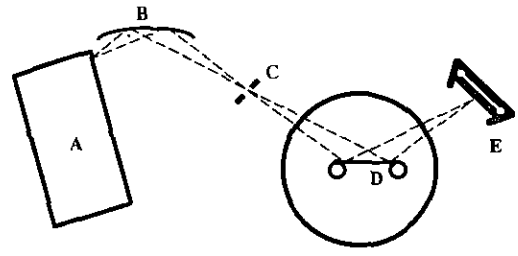

FIG. 1. The X-ray optical system, where (A) is the sealed tube source with a Cu anode; (B) the incident beam focusing monochromator; (C) represents the incident beam slit system; (D) the hot stage and heating strip; and (E) is the PSD.

EXPERIMENTAL SYSTEM AND PROCEDURE

In situ time resolved X-ray diffraction experiments were made with a Siemens D5000 Diffractometer in the vertical $\theta/2\theta$ configuration. Cu$K\alpha_1$ radiation was generated using a 1.5 kW fine-focus sealed-tube source with a curved Ge (111) incident-beam focusing monochromator. This configuration used Bragg–Brentano parafocusing (10). The diffracted intensities were collected with a Braun OED-50M position sensitive detector (PSD) configured to collect intensities simultaneously over a 5.26° 2θ range (Fig. 1). This detector enables data collection roughly one hundred times faster than a standard scintillation detector with similar resolution. To minimize effects of sensitivity variations in the PSD, a Pt sensing wire was used. The detector also scanned continually or oscillated 0.40° 2θ in a "fixed" scan mode to reduce any effects caused by sensitivity variations along the wire (11).

A Bühler HDK 2.3 high-temperature stage ("hot stage") was used to heat the samples under controlled atmospheres. The powder samples were coated on a gold-plated platinum strip 12 mm wide, 5 cm long, and 0.15 mm thick, with a maximum illuminated sample length of 4 mm. A type S (Pt/Pt–10Rh) thermocouple was spot-welded to the heating strip. To minimize the temperature gradient across the sample, it was surrounded by a nearly

cylindrical *environmental heater*, the upper ~30° arc of which was removed to allow unrestricted passage of the X-ray beam. Two concentric thermal radiation shields reduced radiative heat losses to the water-cooled housing.

The composition of the gas phase in the hot stage was monitored by a Dycor MA200M quadrupole gas analyzer. Gas was sampled via a fused silica capillary positioned approximately 10 mm above the sample. The housing, with a volume of 0.8 liters, was purged with the desired gas mixture for a minimum of 5 hr at 200 cm^3/min before the start of an experiment.

The precursor material, prepared by Seattle Specialty Ceramics Inc., was an intimate, homogeneous mixture of $BaCO_3$, CuO, Y_2O_3, and a trace of $Ba(NO_3)_2$. In standard powder diffraction measurements, an infinitely thick sample is used so that the irradiated sample volume does not change with angle. In the high-temperature measurements it was necessary to apply the powder uniformly onto the heating strip while minimizing its thickness to reduce the thermal gradient through the sample. The desired coating was achieved by suspending the precursor powder in absolute ethanol then spraying the mixture onto the heating strip using an artist's airbrush (Paashe VL). An absorption correction then was applied to the intensities obtained from the samples.

Sample emissivity and particle morphology change during the reaction. These factors may introduce an error in estimating the true sample temperature. The environmental heater minimizes the temperature difference between the sample and the surroundings, thereby reducing the error introduced by heat loss. In this experiment the maximum temperature difference between the strip and the environmental heater was 150°C.

The sample was aligned by observing the peak positions of the $BaCO_3$ (111) and (021) reflections. The effective sample thickness can be calculated by comparing the integrated intensity of these reflections to that of the same reflections from an infinitely thick sample. The ratio of the integrated intensities is given by

$$\frac{I}{I_\infty} = 1 - \exp(-2\mu t/\sin\theta), \qquad [7]$$

where μ is the linear absorption coefficient of the precursor powder, and t is the effective sample thickness. For this precursor powder μ is approximately 10^3 cm^{-1}. An effective sample thickness of 0.5 μm was used, with the surface of the film estimated to be less than 10 μm above the strip.

By monitoring the α–β phase transition of K_2CrO_4, which occurs at 674°C (12), an upper bound on the temperature difference across the irradiated section of the sample strip was determined. Over a 10°C temperature range both α and β phases were observed, implying a temperature variation across the sample of ±5°C. A second calibration was made by measuring the lattice parameter of MgO as a function of temperature (12, 13). Magnesium oxide has a cubic structure and isotropic thermal expansion characteristics. A thin, uniform layer of MgO powder was placed on the heating strip. After purging the stage with ultrahigh purity oxygen for two hours, a scan was made at room temperature to determine the lattice constant of the MgO. Subsequently, the temperature was raised and careful diffraction patterns were taken at each temperarure. Each diffraction peak of the MgO was then fitted using a split Pearson VII profile, and the lattice constant a was calculated. The platinum strip deforms slightly at high temperatures, causing a displacement of the sample from the center of the diffractometer. This displacement error causes a shift in the peak position which is given by

$$\Delta(2\theta) = K2\delta\cos\theta, \qquad [8]$$

where K is inversely proportional to the radius of the focusing circle. Using this expression and Bragg's law, the error in lattice constant a becomes

$$\Delta a/a = K'\cot\theta\cos\theta. \qquad [9]$$

The lattice constant was determined by plotting the lattice constant a versus $\cos\theta\cot\theta$ for each Bragg peak at a given temperature and extrapolating this line to $\theta = 90°$. Comparing the lattice constants obtained to those found by Merryman and co-worker (12, 13), we calibrated the thermocouple and determined the sample temperature to within ±5°C.

At the start of each experiment, the powder sample was aligned as described above and the hot stage purged for about 5 hr. The diffractometer collected data in the fixed scan mode, wherein the detector remains stationary over the desired angular range. We were interested in the formation of the 123 phase, as well as any intermediate phases (1–4). The most intense reflections from the 123 phase are the (103) and the (110) which occur at ~32.4° and ~32.8° in 2θ respectively, while for the $BaCu_2O_2$ phase intense reflections occur at 30.8° and 31.2°. Similarly there are intense peaks for the Y_2BaCuO_5 and $BaCuO_2$ phases in angular region of 29–33° 2θ. The reflections shift to lower angles due to thermal expansion, in this case by ~0.5° 2θ. By setting the detector to examine the range 28.5–33.5° 2θ, intense reflections from all the phases were observed. This enabled us to collect data over a short time scale while still maintaining good counting statistics.

A typical high-temperature experiment began with a 60 sec room-temperature fixed scan. The sample was then heated at 20°C/sec to the desired temperature (710°C). Forty successive 60 sec fixed scans were then taken with a 2 sec delay between each scan. Another thirty scans

were made with 30 min delays to allow the reactions to run to completion. The sample was then quenched at a rate of 20°C/sec. By that time, the sample was primarily $YBa_2Cu_3O_6$, so there should have been little change in the phase composition of the sample during the quenching process. No change was observed in test runs. A final room-temperature scan was made over a 80° range in 2θ. This final scan was used for the refinement of mass fractions.

Of the many available Rietveld refinement packages, the General Structure Analysis System (GSAS) (9) proved most suitable to this application. Air scatter contributes strongly to low-angle background intensity collected with a PSD. This package allows the background to be fitted satisfactorily with a cosine series. For each phase present more than thirty parameters need to be refined. To avoid divergence, the variables were slowly added to the refinement. First the overall parameters were varied, such as the scale factors for each phase and the background coefficients. Then parameters were added to the refinement. The order in which these variables were added is very important in order to avoid divergence, so this process was done interactively, allowing only a few iterations between interactions. Variables that appear in the intensity equations with the same functional form should not be refined together. Convergence was reached when the weighted R factor (R_W) was reduced below 0.1 and remained unchanged with subsequent iterations.

The functional form of the Lorentz-polarization correction for data collected with an incident-beam monochromator configuration is not supported by GSAS (14). Data collected from thin powder layers also required a volume-absorption correction. As such, the data were suitably corrected prior to Rietveld refinement. The quality of a refinement was judged by figures of merit which were computed assuming that the accuracy of the X-ray data is governed by $\sqrt{N}$ *counting statistics*. If raw data are modified in any way, their estimated standard deviations (ESDs) had to be corrected by standard error propagation. GSAS allows input of modified ESDs along with corrected raw data. In that way proper figures of merit were obtained.

EXAMPLE

We illustrate the method of kinetic determination by a study of the reaction sequence forming $YBa_2Cu_3O_6$ from $BaCO_3$, Y_2O_3 and CuO in an inert environment, which are (15, 16)

$$CuO + BaCO_3 \rightarrow BaCu_2O_2 + CO_2 + \tfrac{1}{2}O_2 \qquad [10]$$

and

$$Y_2O_3 + 4BaCu_2O_2 + \tfrac{3}{2}O_2 \rightarrow 2YBa_2Cu_3O_6 + 2CuO. \qquad [11]$$

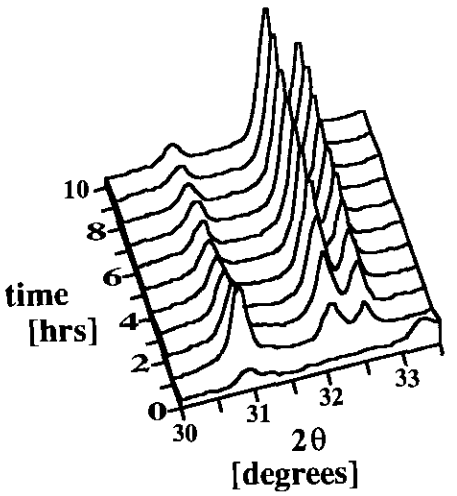

FIG. 2. A series of time-resolved fixed scans of the reacting precursor at 710°C. For purposes of clarity only the scans at hour intervals are shown. The strong reflection at 30.9° 2θ is a barium cuprate reflection while the reflections between 32° and 32.5° are the (103) and (110) reflections of $YBa_2Cu_3O_6$.

In the time-resolved *in situ* measurements, intensities were collected from the $YBa_2Cu_3O_6$ (103) and (110) reflections at 32.2° and 32.6°, and a broad peak at 30.9° which corresponds to the (103) and (200) reflections of $BaCu_2O_2$ (Fig. 2). The $BaCu_2O_2$ and $YBa_2Cu_3O_6$ reflections were fitted with Gaussian profiles, and the background with a straight line, an example of a fixed scan that was fit is

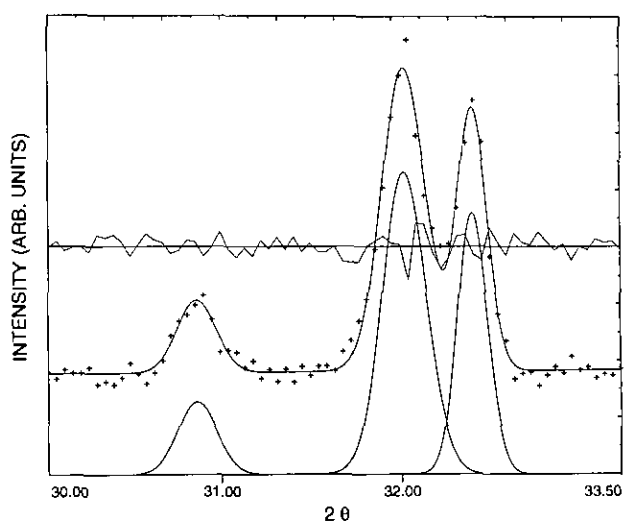

FIG. 3. A fit of a fixed scan, where the hash marks are the raw data and the curve drawn through them is the fit. The continuous curve through the middle of the figure is the difference curve, and the Gaussians are the fitted reflections with the background removed. This fit also allows us to calculate average crystallite dimensions. From this fit we can also show that the crystallites grow faster in the plane than along the c-axis.

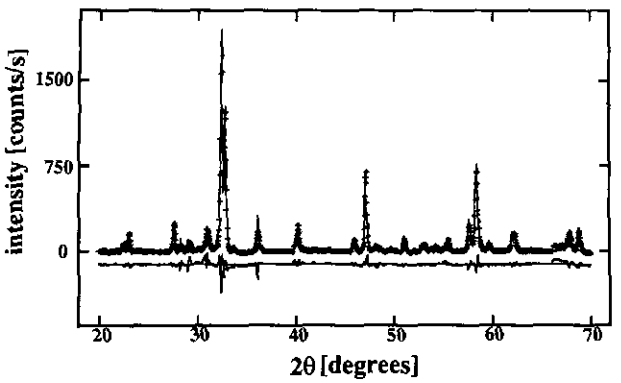

FIG. 4. Rietveld refinement of the final long scan. The hash marks are the data points corrected for the Lorentz-polarization and volume-absorbtion factors, the solid curve is calculated by GSAS, and curve below the data is the difference between the calculated and measured intensities at each point. The angular regions where there are no hash marks (data points) correspond to the substrate reflections that were omitted in this refinement.

shown in Fig. 3. Due to the limited statistics, the profile fitting enabled integrated intensities to be extracted with greater accuracy than by integration performed as a Riemann sum between the peak points and the background. Profile fitting also yields peak widths from which crystallite size can be determined.

A typical Rietveld refinement is shown in Fig. 4. The regions where data are omitted contain substrate reflections that are much more intense than those from $YBa_2Cu_3O_6$. The mass fractions of constituent phases are proportional to the scale factors obtained from GSAS. In the system described by Eqs. [10] and [11] a small mass loss occurs as CO_2 and O_2 evolve. Mass fractions were determined based on the mass of the solids using Eq. [6]. The temporal mass fraction of the $YBa_2Cu_3O_6$ is shown in Fig. 5. This type of information enables one to discriminate among rival kinetic models and to estimate the kinetic parameters of any model.

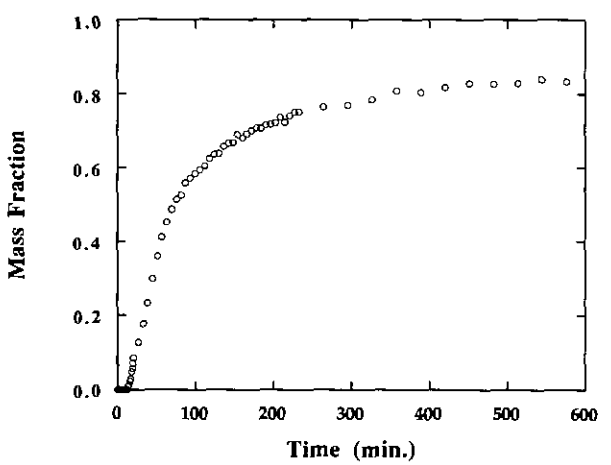

FIG. 5. The temporal mass fraction of $YBa_2Cu_3O_6$ as a function of time at 710°C. The error bars were excluded from this graph, but the errors in the $YBa_2Cu_3O_6$ mass fraction are estimated to be less than 3%.

This technique has some shortcomings. For example, the reaction may not proceed to equilibrium in the duration of the experiment. Crystallite size broadening may cause difficulty distinguishing reflections from background intensity. As a consequence, the mass fractions of phases exhibiting crystallite size broadening are underestimated by the Rietveld refinement. Amorphous phases are also excluded from the refinement. In this work, small crystallites of Y_2O_3 and CuO are present in the quenched samples.

CONCLUSIONS

Time-resolved *in situ* measurements allow continuous monitoring of mass fraction changes during a solid-state reaction and remove the ambiguity of reaction pathways that have plagued traditional measurement techniques. Also, metastable phases, which would not exist in a quenched sample in air, are readily observed. For example, the reduced $BaCu_2O_2$ formed in this process was previously only reported in a formation process *in vacuo* (17).

Determination of mass fractions of a mixture of powders via X-ray diffraction is generally complicated by the differences in structure factors, absorption coefficients, and crystallite size of the different constituent phases. Traditionally this was overcome by adding a known weight percent of a standard powder to the mixture. This is impractical for monitoring a reaction in which the standard may not be inert at elevated temperatures. The technique presented here allows for continuous quantitative monitoring of the mass fraction as a function of time.

ACKNOWLEDGMENTS

This work was supported by the Texas Center for Superconductivity at the University of Houston under a grant from the Department of Defense Advanced Research Projects Agency and the State of Texas. We thank SSC, Inc. for providing the precursor powder used in these studies. We are also grateful to Robert von Dreele, Alan Larson, and David Bish of Los Alamos National Laboratory for their assistance with GSAS. Special thanks to Aaron Herrick for his help in profile fitting.

REFERENCES

1. A. M. Gadalla and T. Hegg, *Thermochim. Acta* **145,** 149 (1989).
2. X. P. Jiang, J. S. Zhang, J. G. Huang, M. Jiang, G. W. Qiao, Z. Q. Hu, and C. X. Shi, *Mater. Lett.* 7(7/8), 250 (1988).
3. N. L. Wu, T. C. Wei, S. Y. Hou, and S. Y. Wong, *J. Mater. Res.* 5, 10, 2056 (1990).
4. E. Ruckenstein, S. Narain, and N. L. Wu, *J. Mater. Res.* 4(2), 267 (1989).
5. H. P. Klug and L. E. Alexander, "X-ray Diffraction Procedures

for Polycrystalline and Amorphous Materials." Wiley, New York, 1974.
6. H. E. Göbel, "Siemens Analytical Applications Note," No. 76. 1985.
7. F. H. Chung, J. Appl. Crystallogr. **8,** 17 (1975).
8. H. M. Rietveld, J. Appl. Crystallogr. **9,** 65 (1969).
9. A. C. Larson and R. B. von Dreele, Computer code GSAS, Los Alamos National Laboratory, 1991.
10. P. D. Garn and O. Menis, "ICTA Certified Differential Thermal Analysis from 125–940°C," p. 15, National Bureau of Standards, Washington, DC, 1971.
11. N. Broll, M. Henne, and W. Krentz, "Siemens Analytical Applications," Note No. 57. 1980.
12. R. G. Merryman, and C. P. Kempter, *J. Am. Ceram. Soc.* **48**(4), 202, (1965).
13. R. G. Merryman, Los Alamos National Laboratory, Report LA-2687, 1964.
14. J. P. Formica, K. Forster, J. T. Richardson, and D. Luss, *in* "Superconductor Engineering" (T. O. Mensah, Ed.). *AIChE Symp. Ser.* **88**(287), 1 (1992).
15. K. M. Forster, J. P. Formica, V. Milonopoulou, J. Kulik, J. T. Richardson, and D. Luss, "Proceedings of the 1992 TcSUH HTS Workshop." 1992.
16. L. V. Azaroff, *Acta Crystallogr.* **8,** 701, (1955).
17. G. S. Grader, P. K. Gallagher, and D. A. Fleming, *Chem. Mater.* **1,** 665 (1989).